

Banner appropriate to article type will appear here in typeset article

Large deformation of elastic capsules under uniaxial extensional flow

Ehud Yariv^{1,2,†}, Peter D. Howell³ and Howard A. Stone²

¹Department of Mathematics, Technion — Israel Institute of Technology, Haifa 32000, Israel

²Department of Mechanical and Aerospace Engineering, Princeton University, Princeton, NJ 08544, USA

³Mathematical Institute, University of Oxford, Oxford OX2 6GG, UK

(Received xx; revised xx; accepted xx)

A spherical capsule (radius R) is suspended in a viscous liquid (viscosity μ) and exposed to a uniaxial extensional flow of strain rate E . The elasticity of the membrane surrounding the capsule is described by the Skalak constitutive law, expressed in terms of a surface shear modulus G and an area dilatation modulus K . Dimensional arguments imply that the slenderness ϵ of the deformed capsule depends only upon K/G and the elastic capillary number $Ca = \mu RE/G$. We address the coupled flow–deformation problem in the limit of strong flow, $Ca \gg 1$, where large deformation allows for the use of approximation methods in the limit $\epsilon \ll 1$. The key conceptual challenge, encountered at the very formulation of the problem, is in describing the Lagrangian mapping from the spherical reference state in a manner compatible with hydrodynamic slender-body formulation. Scaling analysis reveals that ϵ is proportional to $Ca^{-2/3}$, with the hydrodynamic problem introducing a dependence of the proportionality pre-factor upon $\ln \epsilon$. Going beyond scaling arguments, we employ asymptotic methods to obtain a reduced formulation, consisting of a differential equation governing a mapping field and an integral equation governing the axial tension distribution. The leading-order deformation is independent of the ratio K/G ; in particular, we find the approximation $\epsilon^{2/3} Ca \approx 0.2753 \ln(2/\epsilon^2)$ for the correlation between ϵ and Ca . A scaling analysis for the neo-Hookean constitutive law reveals the impossibility of a steady slender shape, in agreement with existing numerical simulations. More generally, the present asymptotic paradigm allows to rigorously discriminate between strain-softening and strain-hardening models.

1. Introduction

Capsules, consisting of a liquid core surrounded by a membrane, are common in both nature (e.g. cells) and bioengineering applications (Pozrikidis 2003b). Since the membrane is elastic, it deforms under flow. Due to the possibility of breakup, there is interest in mechanical modelling of deformation (Barthés-Biesel 2016). In particular, the desire to characterise the mechanical properties of cell membranes has led to the development of deformability cytometry (Otto *et al.* 2015; Mietke *et al.* 2015; Rosendahl *et al.* 2018), where cells are subject to shearing flow in microfluidic devices, with their deformation being recorded by high-speed cameras.

† Email address for correspondence: udi@technion.ac.il

37 It is common to model the thin membrane by a two-dimensional surface with an elastic
38 constitutive law that introduces resistance to shear and area dilation, but not to bending.
39 The canonical problem involves the specification of simple shear flow, under which the
40 membrane deforms. More generally, other types of linear flows have been considered, in
41 particular two-dimensional elongational flow and axially symmetric hyperbolic flow. In
42 these flows, the capsule shape can reach a steady state (which is unattainable under simple
43 shear). For that reason, such flows are convenient for experimental observations and possibly
44 for characterising material response (Chang & Olbricht 1993). With a steady state, moreover,
45 the internal liquid is stationary, so its viscosity does not play a role.

46 The deformed shape of the membrane is determined by static equilibrium, where the
47 hydrodynamic tractions are balanced by the (surface divergence of the) elastic stresses.
48 There is a fundamental difference in determining the hydrodynamic and elastic forces. The
49 hydrodynamic problem, and in particular the resulting traction, is determined by the deformed
50 shape alone. The elastic stresses are set by the deformation from a given reference (typically
51 spherical) shape to the present shape. The theoretical calculation of capsule deformation falls
52 under the broader framework of fluid–structure interactions (Dowell & Hall 2001). Given
53 the typical small size of capsules (e.g. about $10\ \mu\text{m}$ for a red blood cell), inertia is typically
54 negligible; the flow is therefore governed by the Stokes equations.

55 Modelling the elastic response to deformation requires a constitutive law for the stresses.
56 The neo-Hookean law, a particular case of the Mooney–Rivlin law, constitutes the thin limit
57 of an incompressible solid; it appropriately describes rubber-like materials. Another common
58 model is the Skalak law (Skalak *et al.* 1973), an isotropic 2D model with independent surface
59 shear and area dilatation moduli that was specifically designed to model red blood cells. Both
60 constitutive descriptions are nonlinear. With the deformed shape itself being unknown, the
61 equilibrium problem is inherently nonlinear.

62 The key parameter governing the dimensionless problem is the elastic capillary number
63 Ca , representing the characteristic ratio of viscous stresses to elastic stresses close to the
64 reference state. Initial investigations (Barthés-Biesel 1980; Barthés-Biesel & Rallison 1981)
65 considered the stiff limit $Ca \ll 1$, where the membrane deforms only slightly. Given the
66 interest in significant deformations, these were later supplemented by numerical simulations
67 at finite values of Ca (Li *et al.* 1988; Pozrikidis 1990, 2003a; Dodson III & Dimitrakopoulos
68 2008, 2009). The ultimate goal of the theoretical analysis is the calculation of the capsule
69 deformation; representing it by appropriate lumped scalar measures, it is desirable to
70 understand how they vary as a function of Ca .

71 At large Ca the capsule undergoes large deformation whose nature, as observed numerically,
72 depends critically on the elastic behaviour. For certain constitutive laws, the most
73 notable being neo-Hookean, there exists a critical capillary number beyond which no steady
74 shape is attained under elongation (Li *et al.* 1988). For that reason the neo-Hookean law is
75 classified as ‘strain softening.’ For ‘strain hardening’ laws, such as the Skalak description,
76 the capsule does attain a steady slender shape (Li *et al.* 1988; Barthés-Biesel *et al.* 2002;
77 Walter *et al.* 2010). In fact, numerical computations (Dodson III & Dimitrakopoulos 2008,
78 2009) reveal slender shapes even at moderately large Capillary numbers, $Ca \approx 2.5$.

79 Motivated by the interest in large deformation (Eggleton & Popel 1998; Navot 1998;
80 Ramanujan & Pozrikidis 1998) we conduct here an asymptotic investigation in the limit
81 $Ca \gg 1$. Our key goal is to determine the asymptotic dependence of the slenderness ϵ
82 upon Ca . For simplicity we consider uniaxial extensional flow, where the problem is axially
83 symmetric, and seek the steady shape attained by the capsule.

84 In classical slender-body analyses about rigid bodies (Cox 1970; Batchelor 1970) the
85 slenderness $\epsilon \ll 1$ is prescribed in the problem formulation. A key challenge in the present
86 problem is that the slenderness is unknown to begin with, and is in fact a part of the problem.

87 In that sense, our problem is reminiscent of bubble deformation (Buckmaster 1972, 1973;
 88 Acrivos & Lo 1978; Sherwood 1981). It is, however, significantly more complicated. The free
 89 surface in the bubble problem is characterized by a uniform surface tension; consequently,
 90 its mechanical model is expressed via an internal force that acts normal to the surface. The
 91 membrane of a capsule is described by more elaborate mechanics that result in both normal
 92 and tangential internal forces. In that aspect, the present problem is closer to that describing
 93 a bubble whose boundary is contaminated by surfactants (Booty & Siegel 2005). Another
 94 challenge we face, which seems new in slender-body analyses, has to do with the conflict
 95 between the ‘Lagrangian’ description required for the calculation of the elastic stress and the
 96 ‘Eulerian’ description required for the hydrodynamic formulation.

97 In analyzing the deformation problem at large Ca it is necessary to allow for cusped
 98 ends. The transition from spindled-to-cusped edges was originally observed in experiments
 99 (Barthés-Biesel 1991) using a four-roller apparatus (Bentley & Leal 1986). In fact, the
 100 inability of ‘state of the art’ computation schemes (at that time) to reach large capillary
 101 numbers, beyond that transition, motivated the use of spectral boundary-element algorithms
 102 (Wang & Dimitrakopoulos 2006; Dodson III & Dimitrakopoulos 2008) which do predict
 103 cusped ends. In our asymptotic analysis, we allow for pointed ends at the very outset. This
 104 affects the boundary conditions governing the deformed shape.

105 Following the numerical classification of strain softening and strain hardening materials,
 106 we employ here the Skalak model which was numerically observed to result in steady-state
 107 large deformation. Indeed, it seems that the Skalak model has become the *de facto* constitutive
 108 description for capsules in the literature (Dodson III & Dimitrakopoulos 2008, 2009). We also
 109 briefly discuss the strain softening neo-Hookean model, which was numerically observed to
 110 burst under strong flows.

111 2. Problem formulation

112 2.1. Physical problem

113 A capsule is made of a liquid core and an elastic encapsulating membrane, whose reference
 114 shape is spherical, say of radius R . The thin membrane is described by an effective two-
 115 dimensional elasticity which represents resistance to shear (captured by the modulus G) and
 116 area dilatation (captured by the modulus K), but no resistance to bending. The two material
 117 coefficients have the dimensions of surface tension, i.e., force per unit length.

118 The capsule is suspended in a viscous liquid of viscosity μ and is exposed to a uniaxial
 119 extensional flow of extension rate E . The capsule reaches a steady shape whose symmetry
 120 axis is aligned with the axis of extension. The capsule length along that axis is denoted by
 121 $2L$; its ‘waist’ radius in the midway symmetry plane is denoted by ϵL . Our interest is in the
 122 evaluation of the geometric parameters ϵ and L/R , which quantify the overall deformation.
 123 By dimensional arguments, these parameters can only depend upon the two dimensionless
 124 parameters of the problem, namely K/G and the elastic capillary number

$$125 \quad Ca = \frac{\mu RE}{G}, \quad (2.1)$$

126 which expresses the relative magnitude of viscous and elastic stresses. Once the capsule
 127 reaches a steady shape, its core liquid is stationary. The ratio of the core viscosity to the
 128 external-liquid viscosity — a third dimensionless parameter which affects the transient
 129 problem — is accordingly irrelevant.

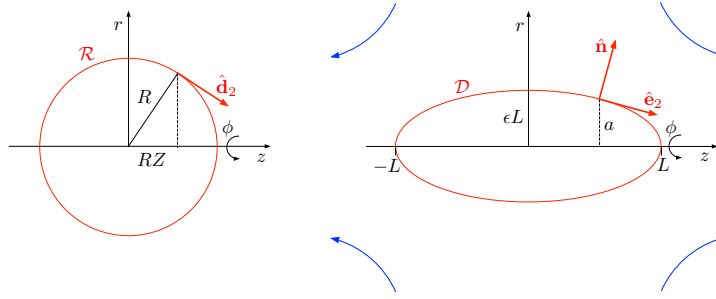


Figure 1: Schematic of the reference (left) and deformed (right) geometries.

130

2.2. Geometry

131 We employ cylindrical (r, ϕ, z) coordinates with the z -axis coinciding with axis of symmetry
 132 and $z = 0$ coinciding with the symmetry plane of the extensional flow. We write the shape
 133 of the deformed membrane \mathcal{D} as

$$134 \quad r = a(z), \quad (2.2)$$

135 see figure 1. Since the deformed shape is symmetric about the plane $z = 0$, a is an even
 136 function: $a(-z) = a(z)$. By definition,

$$137 \quad a(\pm L) = 0. \quad (2.3)$$

138 Given the definition of ϵ , the shape function also satisfies

$$139 \quad a(0) = \epsilon L. \quad (2.4)$$

140 Since the capsule core is incompressible, volume conservation gives the constraint

$$141 \quad \int_{-L}^L a^2(z) dz = \frac{4}{3} R^3. \quad (2.5)$$

142

143 Using z and ϕ for parametrisation, the position vector pointing to the deformed membrane
 144 \mathcal{D} is

$$145 \quad \mathbf{r}(z, \phi) = a(z) \hat{\mathbf{e}}_r + z \hat{\mathbf{e}}_z. \quad (2.6)$$

By differentiating (2.6) we obtain

$$\frac{\partial \mathbf{r}}{\partial \phi} = h_1 \hat{\mathbf{e}}_1, \quad \frac{\partial \mathbf{r}}{\partial z} = h_2 \hat{\mathbf{e}}_2, \quad (2.7a, b)$$

where the associated basis vectors and corresponding scale factors are

$$\hat{\mathbf{e}}_1 = \hat{\mathbf{e}}_\phi, \quad \hat{\mathbf{e}}_2 = \frac{\hat{\mathbf{e}}_z + \hat{\mathbf{e}}_r da/dz}{h_2}, \quad (2.8a, b)$$

and

$$h_1 = a, \quad h_2 = \sqrt{1 + (da/dz)^2}. \quad (2.9a, b)$$

146 The (outward-pointing) unit normal is therefore given by

$$147 \quad \hat{\mathbf{n}} = \hat{\mathbf{e}}_1 \times \hat{\mathbf{e}}_2 = \frac{\hat{\mathbf{e}}_r - \hat{\mathbf{e}}_z da/dz}{h_2}, \quad (2.10)$$

148 see figure 1.

149

2.3. Deformation

In principle, the prescription of the deformation from the reference shape \mathcal{R} to the deformed shape \mathcal{D} requires: (i) parametrisation of \mathcal{R} using two variables; and (ii) mapping each point on \mathcal{R} to a point in \mathcal{D} . Due to the axial symmetry this requires two functions, providing the axial and radial coordinates of the mapped point. Recalling that \mathcal{R} is a sphere of radius R , each point on it is parametrised using its azimuthal coordinate ϕ and its z -coordinate, say RZ ($Z \in [-1, 1]$). The two aforementioned functions, which depend only upon Z , are represented by the mappings:

$$Z \mapsto z, \quad Z \mapsto r. \quad (2.11a, b)$$

150 While this procedure may be suitable to numerical solutions, it does not merge with the
151 eventual need to perform an asymptotic analysis in the slender limit. For example, in analyzing
152 the flow problem the natural parametrisation is expressed in the context of the deformed shape.

153 This incompatibility is resolved using a parametrisation in \mathcal{D} in conjunction with the
154 *inverse* of (2.11a). To that end, we denote the pre-image of z as $Z(z)$. The function $a(z)$,
155 introduced in the previous subsection, is formally constructed by the composition of $Z(z)$
156 with (2.11b).

157 It is evident that $Z(z)$ is an odd function that satisfies

$$158 \quad Z(\pm L) = \pm 1. \quad (2.12)$$

159 It is tempting to add a condition representing the extrema attained by (2.11a) at the two ‘ends’
160 of the capsule. In terms of the mapping $Z(z)$, this gives

$$161 \quad \lim_{|z| \nearrow L} \frac{\sqrt{1-Z^2}}{dZ/dz} = 0. \quad (2.13)$$

162 However, given the anticipation of a cusped-end, we avoid that ‘spindle-end’ condition which
163 only holds for smooth ends. We will provide later the appropriate condition replacing (2.13).

164 Consider now the deformation of a line element corresponding to infinitesimal increments
165 ($d\phi, dz$). The deformation displaces a point with ‘initial’ position

$$166 \quad \mathbf{R}(z, \phi) = \hat{\mathbf{e}}_r R \sqrt{1-Z^2(z)} + \hat{\mathbf{e}}_z R Z(z) \quad (2.14)$$

167 to the ‘new’ position (2.6). Upon differentiating (2.14) we find that

$$168 \quad d\mathbf{R} = \hat{\mathbf{e}}_\phi R \sqrt{1-Z^2} d\phi + \left(\hat{\mathbf{e}}_z - \frac{Z}{\sqrt{1-Z^2}} \hat{\mathbf{e}}_r \right) R \frac{dZ}{dz} dz. \quad (2.15)$$

169 Noting that the two basis vectors in \mathcal{R} are (see figure 1)

$$170 \quad \hat{\mathbf{d}}_1 = \hat{\mathbf{e}}_\phi, \quad \hat{\mathbf{d}}_2 = \hat{\mathbf{e}}_z \sqrt{1-Z^2} - \hat{\mathbf{e}}_r Z, \quad (2.16)$$

171 we find that

$$172 \quad d\mathbf{R} = \hat{\mathbf{d}}_1 R \sqrt{1-Z^2} d\phi + \hat{\mathbf{d}}_2 \frac{R dZ/dz}{\sqrt{1-Z^2}} dz. \quad (2.17)$$

173 Since (2.7) gives

$$174 \quad d\mathbf{r} = \hat{\mathbf{e}}_1 h_1 d\phi + \hat{\mathbf{e}}_2 h_2 dz, \quad (2.18)$$

we can read off the principal stretches, namely

$$\lambda_1 = \frac{a}{R \sqrt{1-Z^2}}, \quad \lambda_2 = \frac{h_2 \sqrt{1-Z^2}}{R dZ/dz}. \quad (2.19a, b)$$

175 Note that λ_1 is the ratio of the deformed radius $a(z)$ to the reference radius at $Z(z)$, see
 176 (2.14).

177 2.4. Flow

Consider now the flow field in the membrane exterior, where the velocity field is denoted by \mathbf{u} and the associated stress tensor by $\boldsymbol{\sigma}$. The flow is governed by the continuity and Stokes equations,

$$\nabla \cdot \mathbf{u} = 0, \quad \nabla \cdot \boldsymbol{\sigma} = \mathbf{0}. \quad (2.20a, b)$$

178 At the deformed membrane it satisfies the no-slip condition,

$$179 \quad \mathbf{u} = \mathbf{0} \quad \text{for} \quad r = a(z), \quad (2.21)$$

180 while at large distances it approaches the imposed flow

$$181 \quad \mathbf{u} \sim E \left(z \hat{\mathbf{e}}_z - \frac{r}{2} \hat{\mathbf{e}}_r \right) \quad \text{as} \quad r^2 + z^2 \rightarrow \infty. \quad (2.22)$$

182 As this is the same problem governing the flow outside a rigid body, the flow is uniquely
 183 determined by the shape of the deformed capsule, as provided by the distribution $a(z)$. Since
 184 the interior fluid is stationary, the stress there is isotropic, say $-PI$.

185 For an incompressible flow, the pressure field is generally defined to within an arbitrary
 186 additive constant; since the pressure difference across the membrane is physically meaningful,
 187 this arbitrariness may only be exploited once, either in the membrane interior or its exterior.
 188 With no loss of generality, we set the pressure at infinity to zero, The constant P thereby
 189 represents the difference between the uniform interior pressure and the far-field pressure in
 190 the exterior region. With that choice, the magnitude of both $\boldsymbol{\sigma}$ and P is proportional to μE ;
 191 in particular, P may be interpreted as a ‘dynamic’ pressure.

192 Due to axial symmetry, the velocity must be of the form

$$193 \quad \mathbf{u} = \hat{\mathbf{e}}_r u + \hat{\mathbf{e}}_z w, \quad (2.23)$$

194 where u and w are functions of r and z , but not of ϕ . Consequently, the Newtonian stress
 195 must be of the form,

$$196 \quad \boldsymbol{\sigma} = \hat{\mathbf{e}}_r \hat{\mathbf{e}}_r \sigma_{rr} + \hat{\mathbf{e}}_z \hat{\mathbf{e}}_z \sigma_{zz} + (\hat{\mathbf{e}}_r \hat{\mathbf{e}}_z + \hat{\mathbf{e}}_z \hat{\mathbf{e}}_r) \sigma_{rz}, \quad (2.24)$$

197 where σ_{rr} , σ_{zz} and σ_{rz} are functions of r and z .

198 2.5. Static equilibrium

199 The shape \mathcal{D} of the deformed membrane is governed by the force balance,

$$200 \quad \nabla_s \cdot \mathcal{T}_s + \hat{\mathbf{n}} \cdot \boldsymbol{\sigma} + \hat{\mathbf{n}} P = \mathbf{0} \quad \text{at} \quad r = a(z), \quad (2.25)$$

201 applying for $-L < z < L$, where ∇_s is the surface-gradient operator and \mathcal{T}_s the surface stress.
 202 By forming the dot product of (2.25) with $\hat{\mathbf{e}}_2$ we obtain the meridional balance,

$$203 \quad \hat{\mathbf{e}}_2 \cdot (\nabla_s \cdot \mathcal{T}_s) + \hat{\mathbf{n}} \cdot \boldsymbol{\sigma} \cdot \hat{\mathbf{e}}_2 = 0. \quad (2.26)$$

204 Similarly, by forming the dot product of (2.25) with $\hat{\mathbf{n}}$ we obtain the normal balance,

$$205 \quad \hat{\mathbf{n}} \cdot (\nabla_s \cdot \mathcal{T}_s) + \hat{\mathbf{n}} \cdot \boldsymbol{\sigma} \cdot \hat{\mathbf{n}} + P = 0. \quad (2.27)$$

206 It is evident from the problem symmetry that the principal directions of the Cauchy tension
 207 \mathcal{T}_s are provided by the unit vectors (2.8). We therefore write the Cauchy tension in the form

$$208 \quad \mathcal{T}_s = \tau_1 \hat{\mathbf{e}}_1 \hat{\mathbf{e}}_1 + \tau_2 \hat{\mathbf{e}}_2 \hat{\mathbf{e}}_2. \quad (2.28)$$

209 The component of $\nabla_s \cdot \mathcal{T}_s$ in the meridional direction is

$$210 \quad \hat{e}_2 \cdot (\nabla_s \cdot \mathcal{T}_s) = \frac{d\tau_2}{ds} + \frac{1}{a} \frac{da}{ds} (\tau_2 - \tau_1), \quad (2.29)$$

211 wherein s is the arc length in the meridional plane, increasing in the direction of \hat{e}_2 ; making
212 use of (2.7b) yields

$$213 \quad \hat{e}_2 \cdot (\nabla_s \cdot \mathcal{T}_s) = \frac{1}{h_2} \left(\frac{d\tau_2}{dz} + \frac{da}{dz} \frac{\tau_2 - \tau_1}{a} \right). \quad (2.30)$$

214 The component of $\nabla_s \cdot \mathcal{T}_s$ in the normal direction is

$$215 \quad \hat{n} \cdot (\nabla_s \cdot \mathcal{T}_s) = \kappa_1 \tau_1 + \kappa_2 \tau_2, \quad (2.31)$$

where the principal curvatures are given by

$$\kappa_1 = -\frac{1}{h_2 a}, \quad \kappa_2 = \frac{1}{h_2^3} \frac{d^2 a}{dz^2}. \quad (2.32a, b)$$

216 Last, making use of (2.8) and (2.10) we find from (2.24) that

$$217 \quad \hat{n} \cdot \sigma \cdot \hat{e}_2 = \frac{[1 - (da/dz)^2] \sigma_{rz} + (da/dz)(\sigma_{rr} - \sigma_{zz})}{h_2^2}, \quad (2.33a)$$

$$218 \quad \hat{n} \cdot \sigma \cdot \hat{n} = \frac{\sigma_{rr} - 2(da/dz)\sigma_{rz} + (da/dz)^2 \sigma_{zz}}{h_2^2}. \quad (2.33b)$$

219 2.6. Axial balance

220 Substituting expressions (2.30) and (2.33a) into the meridional balance (2.26) yields

$$221 \quad \frac{[1 - (da/dz)^2] \sigma_{rz} + (da/dz)(\sigma_{rr} - \sigma_{zz})}{h_2^2} + \frac{1}{h_2} \left(\frac{d\tau_2}{dz} + \frac{da}{dz} \frac{\tau_2 - \tau_1}{a} \right) = 0. \quad (2.34)$$

222 Similarly, substituting (2.31) and (2.33b) into the normal balance (2.27) yields

$$223 \quad \frac{\sigma_{rr} - 2(da/dz)\sigma_{rz} + (da/dz)^2 \sigma_{zz}}{h_2^2} + \kappa_1 \tau_1 + \kappa_2 \tau_2 + P = 0. \quad (2.35)$$

224 Note that (2.34)–(2.35) can be combined to get the axial stress balance

$$225 \quad \frac{d}{dz} (T - \pi a^2 P) = 2\pi a \left(\frac{da}{dz} \sigma_{zz} - \sigma_{rz} \right), \quad (2.36)$$

226 where

$$227 \quad T = \frac{2\pi a \tau_2}{h_2} \quad (2.37)$$

228 is the net axial elastic tension.

229 For a cusped shape we replace (2.13) by the requirement of zero axial tension at the ends
230 of the capsule:

$$231 \quad T(\pm L) = 0. \quad (2.38)$$

232 This condition eliminates the possibility of point singularities at the tips, thus selecting the
233 least-singular solution (Van Dyke 1964). Note that (2.38) is trivially satisfied for rounded
234 ends, where $a \rightarrow 0$ and $|h_2| \rightarrow \infty$ (recall (2.7b)).

2.7. Elasticity

235

236 The evaluation of the Cauchy elastic tension \mathcal{T}_s requires consideration of the elastic
 237 deformation. The principal values of \mathcal{T}_s , $\tau_{1,2}$, are functions of the principal extensional
 238 stretches (4.8). Dimensional arguments for the state of stretch imply that

$$239 \quad \tau_{1,2}/G = \text{functions of } \lambda_1, \lambda_2, K/G. \quad (2.39)$$

Hereafter, we assume the Skalak model (Skalak *et al.* 1973), where

$$\frac{\tau_1}{G} = \frac{\lambda_1 (\lambda_1^2 - 1)}{\lambda_2} + C \lambda_1 \lambda_2 (\lambda_1^2 \lambda_2^2 - 1), \quad \frac{\tau_2}{G} = \frac{\lambda_2 (\lambda_2^2 - 1)}{\lambda_1} + C \lambda_1 \lambda_2 (\lambda_1^2 \lambda_2^2 - 1). \quad (2.40a, b)$$

240 The dimensionless parameter,

$$241 \quad C = \frac{K/G - 1}{2}, \quad (2.41)$$

242 is associated with resistance to area dilation (Barthès-Biesel *et al.* 2002).

243 **3. Strong flow: scaling**

244 Henceforth we focus upon the case of strong flow,

$$245 \quad Ca \gg 1. \quad (3.1)$$

246 In this asymptotic limit, we expect ϵ to be small:

$$247 \quad \epsilon \ll 1. \quad (3.2)$$

248 Our interest is in the dependence of ϵ and L/R upon Ca in the limit (3.1). It is preferable
 249 to temporarily adopt a mathematically equivalent approach where ϵ and L are considered as
 250 known, the former satisfying (3.2). The capillary number Ca and the reference radius R are
 251 then effectively considered as functions of ϵ and L .

Prior to carrying an approximate scheme in the limit (3.2), we perform a scaling analysis. In what follows, we employ \simeq to imply ‘of order.’ In that context, the key estimates are

$$z \simeq L, \quad a \simeq \epsilon L. \quad (3.3a, b)$$

252 It is evident from (2.5) and (3.3) that

$$253 \quad R \simeq L \epsilon^{2/3}. \quad (3.4)$$

We consider first the elastic stresses. Formulae (2.19) for the principal stretches in conjunction with (3.3) imply that $\lambda_1 \simeq \epsilon L/R$ and $\lambda_2 \simeq L/R$. Using (3.4) we find

$$\lambda_1 \simeq \epsilon^{1/3}, \quad \lambda_2 \simeq \epsilon^{-2/3} \quad (3.5a, b)$$

and, consequently, $\lambda_1 \lambda_2 \simeq \epsilon^{-1/3}$. Substitution into (2.40) gives

$$\tau_1 \simeq G \epsilon^{-1}, \quad \tau_2 \simeq G \epsilon^{-7/3}, \quad (3.6a, b)$$

254 so that

$$255 \quad \tau_2 \gg \tau_1, \quad (3.7)$$

256 as would be expected under strong elongation.

It is evident from (2.32) that

$$\kappa_1 \simeq \frac{1}{\epsilon L}, \quad \kappa_2 \simeq \frac{\epsilon}{L}, \quad (3.8a, b)$$

whereby

$$\kappa_1 \tau_1 \simeq GL^{-1} \epsilon^{-2}, \quad \kappa_2 \tau_2 \simeq GL^{-1} \epsilon^{-4/3}, \quad (3.9a, b)$$

257 so, despite (3.7),

$$258 \quad \kappa_1 \tau_1 \gg \kappa_2 \tau_2. \quad (3.10)$$

259 Consider now the divergence of \mathcal{T}_s . It is evident from (2.30) and (3.7) that

$$260 \quad \hat{e}_2 \cdot (\nabla_s \cdot \mathcal{T}_s) \simeq \tau_2 / L. \quad (3.11)$$

261 It also follows from (2.31) and (3.10) that

$$262 \quad \hat{n} \cdot (\nabla_s \cdot \mathcal{T}_s) \simeq \kappa_1 \tau_1. \quad (3.12)$$

Substituting (3.6) and (3.9a) into (3.11)–(3.12) yields

$$\hat{e}_2 \cdot (\nabla_s \cdot \mathcal{T}_s) \simeq GL^{-1} \epsilon^{-7/3}, \quad \hat{n} \cdot (\nabla_s \cdot \mathcal{T}_s) \simeq GL^{-1} \epsilon^{-2}. \quad (3.13a, b)$$

263 With the azimuthal component subdominant, the scaling relation between Ca and ϵ
 264 is determined by the meridional balance (2.26). (In that sense, the present problem is
 265 fundamentally different from the classical problem of a deforming bubble.) To determine
 266 that relation we need to estimate the hydrodynamic stress. We first recall that σ scales as
 267 μE . For small ϵ the shear-stress magnitude is amplified by $1/\epsilon$, so

$$268 \quad \hat{n} \cdot \sigma \cdot \hat{e}_2 \simeq \frac{\mu E}{\epsilon}. \quad (3.14)$$

269 Making use of (3.13a) and (3.14), the meridional balance (2.26) gives

$$270 \quad \frac{G}{L \epsilon^{7/3}} \simeq \frac{\mu E}{\epsilon}. \quad (3.15)$$

271 Making use of (2.1) and (3.4) we obtain the requisite scaling

$$272 \quad Ca \simeq \epsilon^{-2/3}. \quad (3.16)$$

273 For future reference we note from (3.13) that the ratio of $\hat{n} \cdot (\nabla_s \cdot \mathcal{T}_s)$ to $\hat{e}_2 \cdot (\nabla_s \cdot \mathcal{T}_s)$ is
 274 $\simeq \epsilon^{1/3}$.

275 4. Analysis

276 We now go beyond scaling, carrying out a systematic approximation scheme. We retain our
 277 ‘inverted’ approach where ϵ and L are considered as given.

278 4.1. Dimensionless variables

279 At this stage we find it useful to introduce the dimensionless axial coordinate (recall (3.3a)),

$$280 \quad \zeta = z/L. \quad (4.1)$$

281 This induces the definition of the dimensionless mapping $\Psi(\zeta)$,

$$282 \quad Z(z) = \Psi(\zeta), \quad (4.2)$$

283 and the dimensionless shape function $\Phi(\zeta)$ (recall (3.3b))

$$284 \quad a(z) = \epsilon L \Phi(\zeta). \quad (4.3)$$

285 We note that $\Phi(\zeta)$ is an even function while $\Psi(\zeta)$ is an odd function.

In dimensionless form, conditions (2.3) and (2.12) are

$$\Phi(\pm 1) = 0, \quad \Psi(\pm 1) = \pm 1, \quad (4.4a, b)$$

286 while the waist condition (2.4) becomes

$$287 \quad \Phi(0) = 1. \quad (4.5)$$

288 Following (3.4) we define

$$289 \quad R = L\epsilon^{2/3}\chi, \quad (4.6)$$

290 The volume constraint (2.5) thus becomes

$$291 \quad \int_{-1}^1 \Phi^2(\zeta) d\zeta = \frac{4\chi^3}{3}. \quad (4.7)$$

The principal stretches (2.19) become, in terms of Φ and Ψ ,

$$\lambda_1 = \frac{\epsilon L}{R} \frac{\Phi}{\sqrt{1-\Psi^2}}, \quad \lambda_2 = \frac{L}{R} \frac{h_2 \sqrt{1-\Psi^2}}{d\Psi/d\zeta}. \quad (4.8a, b)$$

292 4.2. Approximations for elastic stresses

293 We proceed with a leading-order analysis. In what follows, the symbol ‘ \sim ’ implies ‘asymptotic to,’ with the understanding that the associated error is ‘algebraically small’ (i.e. smaller than
294 some positive power of ϵ).
295

We begin with the geometric quantities. Using (4.1) and (4.3), we see that the scale factors introduced in (2.9) are given by

$$h_1 = \epsilon L \Phi, \quad h_2 \sim 1, \quad (4.9a, b)$$

while the principal curvatures (2.32) become

$$\kappa_1 \sim -\frac{1}{\epsilon L \Phi}, \quad \kappa_2 \sim \frac{\epsilon \Phi}{L}. \quad (4.10a, b)$$

Upon making use of (4.6) and (4.9b), the principal stretches (4.8) simplify to

$$\lambda_1 = \frac{\epsilon^{1/3}}{\chi} \frac{\Phi}{\sqrt{1-\Psi^2}}, \quad \lambda_2 \sim \frac{1}{\epsilon^{2/3}\chi} \frac{\sqrt{1-\Psi^2}}{d\Psi/d\zeta}. \quad (4.11a, b)$$

Consider now the elastic constitutive relations (2.40). Making use of (3.5), we find that they are approximated by

$$\frac{\tau_1}{G} \sim C\lambda_1^3\lambda_2^3, \quad \frac{\tau_2}{G} \sim \frac{\lambda_2^3}{\lambda_1}. \quad (4.12a, b)$$

Substituting (4.11) thus gives

$$\frac{\tau_1}{G} \sim \frac{C}{\chi^6\epsilon} \frac{\Phi^3}{(d\Psi/d\zeta)^3}, \quad \frac{\tau_2}{G} \sim \frac{1}{\chi^2\epsilon^{7/3}} \frac{(1-\Psi^2)^2}{\Phi(d\Psi/d\zeta)^3}. \quad (4.13a, b)$$

296 Consider now the divergence of \mathcal{T}_s . Making use of (2.30) and noting that $\tau_2 \gg \tau_1$ we
297 obtain the meridional component

$$298 \quad \hat{e}_2 \cdot (\nabla_s \cdot \mathcal{T}_s) \sim \frac{1}{a} \frac{d}{dz} (a\tau_2). \quad (4.14)$$

299 Upon substituting (4.1)–(4.3) and (4.13b) we obtain

$$300 \quad \frac{\hat{e}_2 \cdot (\nabla_s \cdot \mathcal{T}_s)}{G/L} \sim \frac{1}{\chi^2\epsilon^{7/3}} \frac{1}{\Phi} \frac{d}{d\zeta} \left[\frac{(1-\Psi^2)^2}{(d\Psi/d\zeta)^3} \right]. \quad (4.15)$$

301 Making use of (2.31) and (3.10) we obtain $\hat{\mathbf{n}} \cdot (\nabla_s \cdot \mathcal{T}_s) \sim \kappa_1 \tau_1$. Substitution of (4.10a)
 302 and (4.13a) gives

$$303 \quad \frac{\hat{\mathbf{n}} \cdot (\nabla_s \cdot \mathcal{T}_s)}{G/L} \sim -\frac{C}{\chi^6 \epsilon^2} \frac{\Phi^2}{(d\Psi/d\zeta)^3}. \quad (4.16)$$

304 The negative sign implies a surface-tension-like ‘inward’ contribution to the normal force
 305 balance.

306 4.3. Flow

307 In the limit (3.2), the flow coincides with that about a slender rigid body (Tillett 1970; Cox
 308 1970; Batchelor 1970). In analyzing flows about rigid bodies, interest typically lies in the
 309 hydrodynamic force acting on the body (or, by extension, in the hydrodynamic couple or
 310 the net stresslet strength). For these quantities, it suffices to determine the distribution of
 311 Stokeslets that represent the body.

312 In the present problem, however, we need the actual shear stress at the boundary of the
 313 body. For that reason, it is desirable to employ an analysis in the spirit of matched asymptotic
 314 expansions, where the Stokeslet distribution represents an approximation on the ‘long’ scale
 315 of body length which is supplemented by a comparable approximation on the ‘short’ cross-
 316 sectional scale ϵ .

317 Given our desire for an algebraically accurate approximation, we prefer to employ the
 318 analysis of Keller & Rubinow (1976), which for the most part avoids an expansion in inverse
 319 powers of $\ln \epsilon$. Adapting their analysis to the present notation, the long-scale flow is written
 320 as a superposition of the ambient flow (2.22) and a collection of Stokeslets (of strength
 321 $\mu EL\mathcal{F}$ per unit length) along the symmetry axis,

$$322 \quad \frac{\mathbf{u}}{EL} \sim \zeta \hat{\mathbf{e}}_z - \frac{\rho}{2} \hat{\mathbf{e}}_r + \frac{1}{8\pi} \int_{-1}^1 \mathcal{F}(\xi) \left\{ \frac{\hat{\mathbf{e}}_z}{[\rho^2 + (\zeta - \xi)^2]^{1/2}} + (\zeta - \xi) \frac{\hat{\mathbf{e}}_r \rho + \hat{\mathbf{e}}_z (\zeta - \xi)}{[\rho^2 + (\zeta - \xi)^2]^{3/2}} \right\} d\xi, \quad (4.17)$$

323 wherein (cf. (4.1))

$$324 \quad \rho = r/L. \quad (4.18)$$

325 On the cross-sectional scale, where $\rho = O(\epsilon)$, the flow is primarily in the axial direction.
 326 Thus, making use of the form (2.23), $w/EL = O(1)$ while u/EL is $O(\epsilon)$. In particular,
 327 imposing the no slip condition at $\rho/\epsilon = \Phi$ and compatibility with (4.17) yields (see equations
 328 (1), (2) and (9) in Keller & Rubinow (1976))

$$329 \quad \frac{w}{EL} \sim -\frac{\mathcal{F}(\zeta)}{2\pi} \ln \frac{\rho}{\epsilon\Phi(\zeta)}. \quad (4.19)$$

330 The integral equation governing the Stokeslet distribution $\mathcal{F}(\zeta)$ was determined by Keller &
 331 Rubinow (1976) via matching between the long-scale and short-scale solutions (see Eq. (12)
 332 in Keller & Rubinow (1976)). Adapting to the present notation, this equation reads

$$333 \quad 4\pi\zeta + [\ln(1 - \zeta^2) - 1]\mathcal{F}(\zeta) + \int_{-1}^1 \frac{\mathcal{F}(\xi) - \mathcal{F}(\zeta)}{|\xi - \zeta|} d\xi = 2\mathcal{F}(\zeta) \ln \frac{\epsilon\Phi(\zeta)}{2}. \quad (4.20)$$

334 Consistently with our approach (and, more generally, with established asymptotic practices
 335 (Fraenkel 1969)), we retain terms that are logarithmically small in ϵ while neglecting
 336 algebraically small corrections.

337 We can now calculate the hydrodynamic shear stress in terms of \mathcal{F} . It is evident that on the
 338 cross-sectional scale $\sigma_{rz} \sim \mu \partial w / \partial r$. Substituting (4.18) and (4.19) we obtain the $O(\epsilon^{-1})$

339 stress (cf. (3.14)),

$$340 \quad \sigma_{rz}/\mu E \sim -\frac{\mathcal{F}(\zeta)}{2\pi\epsilon\Phi(\zeta)} \quad \text{at} \quad \rho = \epsilon\Phi(\zeta). \quad (4.21)$$

It is readily verified that both $\sigma_{rr}/\mu E$ and $\sigma_{zz}/\mu E$ are $O(1)$ on the cross-sectional scale. From (2.33a)–(2.33b) we then conclude that

$$\frac{\hat{\mathbf{n}} \cdot \boldsymbol{\sigma} \cdot \hat{\mathbf{e}}_2}{\mu E} \sim -\frac{\mathcal{F}(\zeta)}{2\pi\epsilon\Phi(\zeta)}, \quad \frac{\hat{\mathbf{n}} \cdot \boldsymbol{\sigma} \cdot \hat{\mathbf{n}}}{\mu E} = O(1). \quad (4.22a, b)$$

341

4.4. Dominant balances

342 Requiring that the two terms in meridional equilibrium (2.26) balance, we find using (4.15)
343 and (4.22a)

$$344 \quad \frac{G/L}{\chi^2 \epsilon^{7/3}} \frac{d}{d\zeta} \left[\frac{(1-\Psi^2)^2}{(d\Psi/d\zeta)^3} \right] \sim \frac{\mu E \mathcal{F}}{2\pi\epsilon} \quad (4.23)$$

345 Making use of (2.1) and (4.6) we obtain

$$346 \quad 2\pi \frac{d}{d\zeta} \left[\frac{(1-\Psi^2)^2}{(d\Psi/d\zeta)^3} \right] \sim Ca \chi \epsilon^{2/3} \mathcal{F}. \quad (4.24)$$

347 Thus, Ca scales as $\epsilon^{-2/3}$, as already anticipated in (3.16). Defining the rescaled capillary
348 number

$$349 \quad \widetilde{Ca} = Ca \chi \epsilon^{2/3} \quad (4.25)$$

350 we obtain

$$351 \quad \frac{d\Omega}{d\zeta} \sim \widetilde{Ca} \mathcal{F}(\zeta), \quad (4.26)$$

352 wherein

$$353 \quad \Omega(\zeta) = 2\pi \frac{(1-\Psi^2)^2}{(d\Psi/d\zeta)^3} \quad (4.27)$$

354 is a (leading-order) dimensionless version of the axial tension (2.37):

$$355 \quad \Omega = \epsilon^2 \chi^3 \frac{T}{GR}. \quad (4.28)$$

356 Consider now the normal balance (2.27). It follows from (2.1), (4.6), (4.16) and (4.22b) that
357 the ratio of $\hat{\mathbf{n}} \cdot \boldsymbol{\sigma} \cdot \hat{\mathbf{n}}$ to $\hat{\mathbf{n}} \cdot (\nabla_s \cdot \mathcal{T}_s)$ is of order $Ca \epsilon^{4/3}$, or, using (3.16), of order $\epsilon^{2/3}$. This was
358 to be expected: we already saw from the scaling estimate (3.13) that the normal component
359 of $\nabla_s \cdot \mathcal{T}_s$ is $O(\epsilon^{1/3})$ relative to meridional component. The hydrodynamic considerations, on
360 the other hand, revealed that the ratio of the normal Newtonian stress to the shear Newtonian
361 stress is of order ϵ . It follows that the hydrodynamic traction does not participate at the
362 dominant balance of (2.27), which must therefore involve the elastic force (4.16) and the core
363 pressure. Defining the dimensionless pressure

$$364 \quad \Pi = \frac{P}{\mu E}, \quad (4.29)$$

365 we therefore obtain

$$366 \quad \frac{G}{L} \frac{C}{\chi^6 \epsilon^2} \frac{\Phi^2}{(d\Psi/d\zeta)^3} \sim \mu E \Pi. \quad (4.30)$$

367 Making use of (2.1), (4.6) and (4.25) yields the dimensionless balance

$$368 \quad \frac{\Phi^2}{(d\Psi/d\zeta)^3} \sim \epsilon^{2/3} \frac{\chi^4 \widetilde{Ca}}{C} \Pi. \quad (4.31)$$

369 It follows that Π scales as $\epsilon^{-2/3}$ — namely as the capillary number. Defining the rescaled
370 pressure,

$$371 \quad \widetilde{\Pi} = \epsilon^{2/3} \frac{\chi^4 \widetilde{Ca}}{C} \Pi, \quad (4.32)$$

372 we find that (4.31) is simplified to

$$373 \quad \Phi = \widetilde{\Pi}^{1/2} \left(\frac{d\Psi}{d\zeta} \right)^{3/2}, \quad (4.33)$$

374 where we used the fact that both Φ and $d\Psi/d\zeta$ are non-negative.

375 5. Reduced problem

376 We now summarise the reduced problem governing the mapping Ψ and the tension Ω
377 introduced in (4.27). The relation (4.27) is rewritten as a first-order differential equation,

$$378 \quad \frac{d\Psi}{d\zeta} = (2\pi)^{1/3} \frac{(1 - \Psi^2)^{2/3}}{\Omega^{1/3}}. \quad (5.1)$$

379 The shape is obtained from (4.33) and (5.1)

$$380 \quad \Phi = (2\pi \widetilde{\Pi})^{1/2} \frac{1 - \Psi^2}{\Omega^{1/2}}. \quad (5.2)$$

381 Substituting (4.26) and (5.2) into (4.20), we obtain

$$382 \quad 4\pi \widetilde{Ca} \zeta + [\ln(1 - \zeta^2) - 1] \Omega'(\zeta) + \int_{-1}^1 \frac{\Omega'(\xi) - \Omega'(\zeta)}{|\xi - \zeta|} d\xi = \Omega'(\zeta) \ln \frac{\epsilon^2 \pi \widetilde{\Pi} (1 - \Psi^2)}{2\Omega}, \quad (5.3)$$

383 where the prime denotes differentiation. The deformation problem is therefore governed by
384 the set (5.1) and (5.3).

385 Since $\Psi(\zeta)$ is an odd function, $\Omega(\zeta)$ must be even: see (4.27). We therefore solve only for
386 $\zeta > 0$, replacing (5.3) by

$$387 \quad \Omega'(\zeta) \ln \frac{\epsilon^2 \pi \widetilde{\Pi} (1 - \Psi^2)}{2\Omega} - 4\pi \widetilde{Ca} \zeta$$

$$388 \quad = [\ln(1 - \zeta^2) - 1] \Omega'(\zeta) + \int_0^1 \frac{\Omega'(\xi) - \Omega'(\zeta)}{|\xi - \zeta|} d\xi - \int_0^1 \frac{\Omega'(\xi) + \Omega'(\zeta)}{|\xi + \zeta|} d\xi, \quad (5.4)$$

and adding the symmetry conditions

$$\Omega'(0) = 0, \quad \Psi(0) = 0. \quad (5.5a, b)$$

389 These are supplemented by the end condition,

$$390 \quad \Psi(1) = 1, \quad (5.6)$$

391 which follows from (4.4) and (5.2); the waist condition

$$392 \quad \Omega(0) = 2\pi \widetilde{\Pi}, \quad (5.7)$$

393 which follows from (4.5) and (5.2); and the tip condition,

$$394 \quad \Omega(1) = 0, \quad (5.8)$$

395 which constitutes the dimensionless version of (2.38).

396 We note that (5.5a) is trivially satisfied by (5.4). Thus, equations (5.1) and (5.4) together
 397 with the four conditions (5.5b)–(5.8) presumably provide a closed system for $\Omega(\zeta)$ and $\Psi(\zeta)$,
 398 in which the dimensionless parameters \widetilde{Ca} and $\widetilde{\Pi}$ are determined as part of the solution.
 399 Conveniently, the above problem is independent of χ . Once the problem has been solved, χ
 400 may be determined from the relation

$$401 \quad \pi \widetilde{\Pi} \int_0^1 \frac{(1 - \Psi^2)^2}{\Omega} d\zeta = \frac{\chi^3}{3}, \quad (5.9)$$

402 which follows from (4.7) in conjunction with (5.2). The dimensionless capsule length and
 403 capillary number corresponding to the chosen value of ϵ are then recovered from (4.6) and
 404 (4.25), respectively.

405 We note that the reduced problem is independent of C . Once the problem is solved and $\widetilde{\Pi}$
 406 is calculated, the value of C affects the core pressure Π , see (4.32). Otherwise, C does not
 407 affect the capsule shape at the present leading-order approximation scheme.

408 6. Logarithmic approximation

409 Let us derive a ‘logarithmically accurate’ approximation by considering $\ln(2/\epsilon^2)$ as being
 410 asymptotically large. It is evident that the leading-order balance in (5.4) takes place between
 411 the two terms in the left-hand side. We can therefore make the leading-order approximation

$$412 \quad \frac{d\Omega}{d\zeta} \approx -\frac{4\pi \widetilde{Ca} \zeta}{\ln(2/\epsilon^2)}, \quad (6.1)$$

413 where the symbol ‘ \approx ’ is used to represent the ‘logarithmic’ approximation.

414 We can immediately integrate (6.1) and apply the tip condition (5.8) to get the leading-order
 415 tension

$$416 \quad \Omega(\zeta) \approx \frac{2\pi \widetilde{Ca} (1 - \zeta^2)}{\ln(2/\epsilon^2)}, \quad (6.2)$$

417 whereby condition (5.7) yields

$$418 \quad \widetilde{\Pi} \approx \frac{\widetilde{Ca}}{\ln(2/\epsilon^2)}. \quad (6.3)$$

419 From (5.1) we then obtain the separable equation,

$$420 \quad \frac{\widetilde{\Pi}^{1/3}}{(1 - \Psi^2)^{2/3}} \frac{d\Psi}{d\zeta} \approx \frac{1}{(1 - \zeta^2)^{1/3}}, \quad (6.4)$$

421 which may be immediately integrated to give

$$422 \quad \widetilde{\Pi}^{1/3} \Psi {}_2F_1\left(\frac{1}{2}, \frac{2}{3}, \frac{3}{2}; \Psi^2\right) \approx \zeta {}_2F_1\left(\frac{1}{3}, \frac{1}{2}, \frac{3}{2}; \zeta^2\right), \quad (6.5)$$

423 in which ${}_2F_1$ is a hypergeometric function, and the integration constant vanishes because of
 424 condition (5.5b).

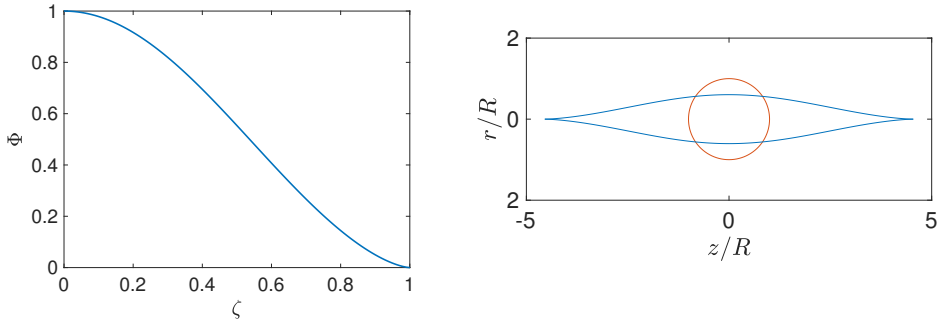


Figure 2: Logarithmic approximation: (a) Universal shape: Φ versus ζ . (b) Physical shape in the $(r/R, z/R)$ coordinates for $Ca = 5$.

425 Application of (5.6) gives

$$426 \quad \tilde{\Pi} \approx \left[\frac{{}_2F_1\left(\frac{1}{3}, \frac{1}{2}, \frac{3}{2}; 1\right)}{{}_2F_1\left(\frac{1}{2}, \frac{2}{3}, \frac{3}{2}; 1\right)} \right]^3 = \frac{\pi^{3/2}[\Gamma(5/6)]^3}{54[\Gamma(7/6)]^6}. \quad (6.6)$$

427 By expanding (6.5) near $\zeta = 1$ and $\Psi = 1$ we obtain, using (6.6),

$$428 \quad \Psi(\zeta) \sim 1 - \frac{\pi^{3/2}[\Gamma(7/6)]^3}{2[\Gamma(5/6)]^6} (1 - \zeta)^2 \quad \text{as } \zeta \nearrow 1. \quad (6.7)$$

429 Given (6.6), the implicit relation (6.5) provides Ψ as a function of ζ , independent of ϵ .
430 Substituting (6.2)–(6.3) into (5.2) yields the shape

$$431 \quad \Phi = \frac{1 - \Psi^2}{(1 - \zeta^2)^{1/2}}. \quad (6.8)$$

432 Note that (6.7)–(6.8) implies that Φ behaves like $(1 - \zeta)^{3/2}$ as $\zeta \nearrow 1$, consistently with the
433 assumption of a cusp. The universal shape, as obtained from substitution of (6.5)–(6.6) into
434 (6.8), is shown in figure 2(a).

435 The volume constraint (5.9) reads here

$$436 \quad \int_0^1 \frac{(1 - \Psi^2)^2}{1 - \zeta^2} d\zeta = \frac{2\chi^3}{3}, \quad (6.9)$$

437 independently of ϵ . Evaluation using the universal function provided by (6.5) and (6.6) yields

$$438 \quad \chi = 0.8448 \dots \quad (6.10)$$

439 The capsule length is obtained from (4.6) as

$$440 \quad L/R \approx 1.1837\epsilon^{-2/3}, \quad (6.11)$$

441 while evaluation of (6.6) gives

$$442 \quad \tilde{\Pi} = 0.2326 \dots \quad (6.12)$$

443 The capillary number is obtained from (4.25), which upon using (6.3), (6.10) and (6.12)
444 gives

$$445 \quad Ca \approx 0.2753 \epsilon^{-2/3} \ln(2/\epsilon^2). \quad (6.13)$$

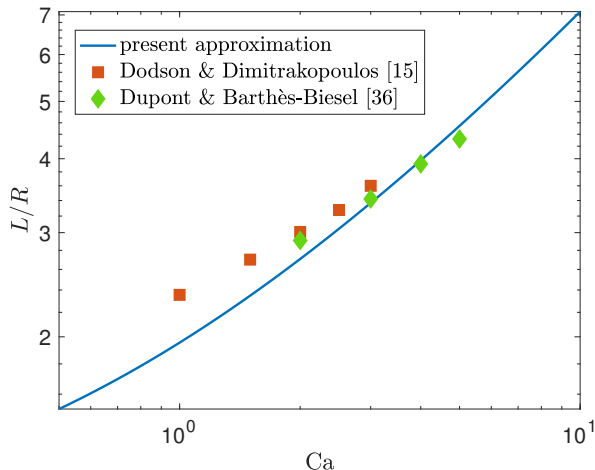


Figure 3: L/R as a function of Ca . Solid: logarithmic approximation, (6.11) and (6.13). Squares: data set from [Dodson III & Dimitrakopoulos \(2009\)](#). Diamonds: data set from [Dupont & Barthès-Biesel \(2024\)](#).

446 With the universal shape $\Phi(\zeta)$ available, we may employ (4.1), (4.3) and (6.11) to plot the
 447 ‘physical shape’ of the capsule on the length scale R for a given capillary number, with the
 448 slenderness ϵ determined from (6.13). In figure 2(b) we plot that physical shape for $Ca = 5$.
 449 The reference spherical shape is also shown.

450 In comparing our approximation with the existing literature we employ two sets of data
 451 points, both obtained for the Skalak law (2.40) with $C = 1$. The first is obtained from
 452 the numerical simulations of [Dodson III & Dimitrakopoulos \(2009\)](#). While these authors
 453 consider planar hyperbolic flow, it is plausible that these results are quantitatively similar
 454 to those of uniaxial flow: indeed, [Hinch & Acrivos \(1979\)](#) analysed bubble deformation in
 455 planar flow by viewing it as a perturbation of the axisymmetric case. By interpolating from
 456 figure 16 in [Dodson III & Dimitrakopoulos \(2009\)](#), we obtained values of L/R for the Ca
 457 values 1, 1.5, 2, and 2.5; in addition, [Dodson III & Dimitrakopoulos \(2009\)](#) cite the value
 458 $L/R = 3.6$ for $Ca = 3$. The second set was kindly provided by [Dupont & Barthès-Biesel](#)
 459 [\(2024\)](#) who recently performed numerical simulations of the present problem. We used their
 460 results for the Ca values 2, 3, 4 and 5. Note that the physical shape in figure 2(b) has been
 461 portrayed for their maximal value of Ca .

462 The comparison is shown in figure 3 where the theoretical approximation for L/R as a
 463 function of Ca is obtained from (6.11) and (6.13). Given the crude nature of the logarithmic
 464 approximation and the rather modest Ca -values which have been employed in the simulations,
 465 the agreement is gratifying.

466 7. Neo-Hookean membranes

467 The preceding analysis was carried out for an elastic membrane governed by the Skalak
 468 constitutive description. In principle, it can be carried out for other elastic models, provided
 469 the membrane reaches a steady state under large deformation.

In fact, the very possibility of steady state can be inferred from a scaling analysis akin to
 that carried out in §3. As an illustration, consider the neo-Hookean model ([Barthès-Biesel](#)

et al. 2002) where (2.40) is replaced by

$$\frac{\tau_1}{G} = \frac{\lambda_1}{\lambda_2} - \frac{1}{\lambda_1^3 \lambda_2^3}, \quad \frac{\tau_2}{G} = \frac{\lambda_2}{\lambda_1} - \frac{1}{\lambda_1^3 \lambda_2^3}. \quad (7.1a, b)$$

Making use of (3.5), we find that the stress estimates (3.6) are replaced by

$$\tau_1 \simeq G\epsilon, \quad \tau_2 \simeq G\epsilon^{-1}, \quad (7.2a, b)$$

470 while the estimates (3.9) are replaced by

$$471 \quad \kappa_1 \tau_1, \kappa_2 \tau_2 \simeq GL^{-1}. \quad (7.3)$$

472 Since (3.11) still holds, we find using (7.2b) that (3.13a) is replaced by

$$473 \quad \hat{\boldsymbol{e}}_2 \cdot (\nabla_s \cdot \mathcal{T}_s) \simeq GL^{-1} \epsilon^{-1}. \quad (7.4)$$

474 Also, from (2.31) and (7.3) it follows that (3.13b) is replaced by

$$475 \quad \hat{\boldsymbol{n}} \cdot (\nabla_s \cdot \mathcal{T}_s) \simeq GL^{-1}. \quad (7.5)$$

476 Thus, just like in the Skalak model, $\hat{\boldsymbol{e}}_2 \cdot (\nabla_s \cdot \mathcal{T}_s) \gg \hat{\boldsymbol{n}} \cdot (\nabla_s \cdot \mathcal{T}_s)$. Balancing (7.4) with (3.14),
477 the meridional balance (2.26) gives (cf. (3.15))

$$478 \quad \frac{G}{L\epsilon} \simeq \frac{\mu E}{\epsilon} \quad (7.6)$$

479 Making use of (2.1) and (3.4) we obtain the scaling

$$480 \quad Ca \simeq \epsilon^{2/3}, \quad (7.7)$$

481 which contradicts (3.2). This indicates the impossibility of a steady slender shape. Our
482 conclusion is compatible with the numerical simulations of Barthès-Biesel *et al.* (2002),
483 who observed that a neo-Hookean capsule stretches indefinitely in an elongational flow.

484 The key to a possible slender limit is the need for the elastic stresses to increase sufficiently
485 fast with diminishing ϵ so as to overcome the viscous stress that grows as ϵ^{-1} , see (3.14). For
486 a given reference radius R , the meridional components of $\nabla_s \cdot \mathcal{T}_s$ increases with diminishing
487 ϵ in both the Skalak and neo-Hookean models, but at quite different rates. In the Skalak
488 model, it scales as $\epsilon^{-5/3}$ (recall (3.4) and (3.13a)), thus giving rise to the scaling relation
489 (3.16) which is compatible with (3.2). In the neo-Hookean model, it scales as $\epsilon^{-1/3}$ (see (3.4)
490 and (7.4)); since the modest growth rate with diminishing ϵ does not overcome that in (3.14),
491 the resulting scaling (7.7) is incompatible with the slenderness assumption (3.2).

492 The scaling analyses in the present paper thus provide a rigorous manner to discriminate
493 between strain-softening and strain-hardening models.

494 8. Discussion

495 As a preliminary to the discussion, we provide two tables which could help the reader identify
496 the key quantities. Table 1 describes the pertinent coordinates and fields. Table 2 describes
497 the dimensionless parameters.

498 Using slender-body approximations, we derived a reduced model governing the deformation
499 of an elastic capsule in a strong hyperbolic straining flow. The asymptotic description
500 consists of the integral equation (5.3) and the first-order differential equation (5.1). The
501 former may be considered as an equation governing the tension Ω ; the latter as an equation
502 governing the mapping Ψ relating the reference and present membrane geometries.

503 Interpreting these equations as two first-order ordinary differential equations, their solution

Original	Rescaled	Description	Reference
z	ζ	axial coordinate	(4.1)
r	ρ	radial coordinate	(4.18)
a	Φ	cross-sectional radius	(4.3)
Z	Ψ	inverse map	(4.2)
T	Ω	cross-sectional tension	(4.28)

Table 1: Coordinates and fields: original (dimensional, except Z) and rescaled (dimensionless).

Parameter	Description	Reference
Ca	capillary number	(2.1)
ϵ	slenderness	(2.4)
L/R	axial elongation	(2.3)
C	resistance to dilatation	(2.41)
χ	related to L/R	(4.6)
\widetilde{Ca}	rescaled capillary number	(4.25)
$\widetilde{\Pi}$	core pressure	(4.29)
$\widetilde{\Pi}$	rescaled core pressure	(4.32)

Table 2: Dimensionless parameters.

504 introduces two integration constants. Since these equations also involve the two unknown
505 parameters \widetilde{Ca} and $\widetilde{\Pi}$, four auxiliary conditions are required. These are provided by (5.5b)–
506 (5.8). Of the original six conditions, (5.5a) is trivially satisfied while the two conditions
507 $\Phi(1) = 0$ and $\Psi(1) = 1$ are not independent because of (5.2).

508 It is important to emphasize, however, that all the original six conditions are required
509 when ϵ is not small. This is compatible with the effective reduction of order that takes place
510 in the limit $\epsilon \rightarrow 0$. Indeed, with κ_2 algebraically small compared with κ_1 (recall (4.10)),
511 the second derivative of Φ does not appear in the reduced problem. The reduction of order
512 suggests that the scale disparity (3.8) should fail in a neighborhood of the capsule tips, where
513 the highest-derivative term in κ_2 must come into play. For the case of an inviscid bubble,
514 Buckmaster (1972) speculates that slender-body theory breaks down in a region near the tips
515 that is exponentially small in ϵ , and the same may be true in our case. It is also possible that
516 our approximation becomes non-uniform near the equator, where the assumption of strong
517 flow breaks down (Acrivos & Lo 1978).

518 The end goal of our contribution has been the calculation of the capsule deformation,
519 and in particular its lumped description by the scalar quantities ϵ and L/R . Our analysis
520 has additionally provided asymptotic information on the elastic stress system created by the
521 imposed elongation. We here wish to address two aspects of that system, both associated
522 with the parameter C , as given by (2.41).

523 The first has to do with the possibility of buckling. If the azimuthal stress is compressive
524 ($\tau_1 < 0$) the axisymmetric shape may become unstable, resulting in a cross-sectional
525 buckling. This symmetry breaking cannot be captured by (numerical or asymptotic) models
526 that are predicated upon axial symmetry. In the present asymptotic description, τ_1 is given
527 by (4.13a), representing a situation where the first term on the right-hand side of (2.40a) is

528 subdominant. While C is strictly $> -1/2$, it is universally considered non-negative in the
 529 literature. (For example, [Barthès-Biesel *et al.* \(2002\)](#) considered the C values 0, 1, 10 and
 530 100.) With (4.13a) being non-negative for $C \geq 0$, our axisymmetric profiles are stable. This
 531 observation agrees with the (fully three-dimensional) numerical simulations of [Dupont &
 532 Barthès-Biesel \(2024\)](#), carried out for $C = 1$, which predict buckling only for small values
 533 of Ca .

534 The second observation has to do with the limit of large C . The terms proportional to C in
 535 (2.40) are associated with resistance to area dilatation. Indeed, nearly inextensible membranes
 536 (e.g. lipid bilayers) have been analysed in the literature assuming $C \gg 1$ ([Skalak *et al.* 1973](#)).
 537 It may appear as though the limit $C \gg 1$ in the present description merely results in a core
 538 pressure that is much larger than $\epsilon^{-2/3}$ (recall (4.32)). However, the underlying approximation
 539 (4.12b) breaks down for $C = O(\epsilon^{-4/3})$, when the second term in the right-hand side of (2.40b)
 540 is no longer subdominant.

541 9. Concluding remarks

542 We have addressed the deformation of a Skalak capsule under strong uniaxial elongation. The
 543 desire to employ slender-body theory has been impeded by two obstacles. The first is that the
 544 slender geometry, and in particular the slenderness ϵ , is unknown to begin with. This obstacle
 545 is quite familiar from classical analyses of deformable bubbles in such flows ([Buckmaster
 546 1972, 1973](#); [Acivos & Lo 1978](#); [Sherwood 1981](#)) as well as comparable investigations of both
 547 hydrostatic ([Sherwood 1991](#); [Stone *et al.* 1999](#); [Rhodes & Yariv 2010](#)) and hydrodynamic
 548 ([Dubash & Mestel 2007](#); [Yariv & Rhodes 2013](#)) deformations under an electric field. It is
 549 handled by temporarily considering the shape to be known. The second obstacle, unique to
 550 membrane deformation, has to do with the intrinsic conflict between Lagrangian and Eulerian
 551 descriptions. In the present contribution, it was tackled by via the use of the inverse of the
 552 standard mapping from the reference state.

553 The slender-body *ansatz* allows to obtain elementary approximations for the elastic stresses
 554 in the membrane. Making use of the paradigm of [Keller & Rubinow \(1976\)](#), it also provides
 555 closed-form approximations for the hydrodynamic stresses. This approach eventually results
 556 in a reduced problem, consisting of equations (5.1) and (5.4) and conditions (5.5b)–(5.8),
 557 governing two functions of the axial coordinate. The first is the net cross-sectional tension;
 558 the second is the above-mentioned inverse map. The asymptotic error in the reduced problem
 559 is algebraically small in ϵ (and therefore also in Ca). In solving it, however, we employed
 560 a ‘logarithmic’ approximation, neglecting terms of order $1/\ln \epsilon$. The shape prediction of
 561 the resulting closed-form solution is in surprising agreement with numerical results in the
 562 literature, obtained at rather mild values of the capillary number.

563 It would be of interest to solve the reduced problem numerically ([Tornberg & Shelley 2004](#))
 564 and compare the results, where the asymptotic error is ensured to be algebraically small,
 565 to the logarithmic approximation derived herein. Another natural direction is motivated by
 566 the experimental observation of capsule breakup in strong flows ([Barthès-Biesel 1991](#)): for
 567 a given lytic tension, one could use the asymptotic results in the present contribution as a
 568 basis for rupture prediction ([Dodson III & Dimitrakopoulos 2009](#)), possibly allowing the
 569 identification of a critical capillary number. Also, given the instabilities that are encountered
 570 in numerical simulations, it is desirable to use the steady shape identified in the present
 571 contribution as a basis for a stability calculation, possibly allowing the identification of a
 572 critical capillary number.

573 Otherwise, future extensions of the present work fall into three categories. The first involves
 574 the limit of large capillary numbers with nearly inextensible membranes. As observed in §8,
 575 our asymptotic analysis breaks down when C becomes comparable to $\epsilon^{-4/3}$. Assuming that

576 the scaling (3.16) is retained, this suggests the analysis of the distinguished limit where Ca
 577 and C are large with $C^{1/2}/Ca$ fixed.

578 The second category entails the same flow problem with a more sophisticated membrane
 579 model (Barthés-Biesel 2016). Perhaps the most important modification is the introduction of
 580 a small resistance to bending which necessarily follows from the small but finite membrane
 581 thickness. This modification is expected to be significant near the tips, where it excludes the
 582 possibility of cusped ends.

583 The third category involves the consideration of different ambient flows. Perhaps the most
 584 important direction in that category is the consideration of planar extensional flow. This flow
 585 has been ubiquitous in theoretical analysis (Dodson III & Dimitrakopoulos 2009), perhaps
 586 because of feasibility of simple experimental realisation via a four-roller mill setup (Bentley
 587 & Leal 1986). Since it results in a steady state, it is simpler to analyse than, say, shear flow.
 588 Nonetheless, the resulting problem is more challenging than the present one as it does not
 589 possess axial symmetry. In particular, the cross sectional shape is not circular. This requires
 590 a more sophisticated use of slender-body theory (Batchelor 1970; Borker & Koch 2019).

591 **Declaration of Interests.** The authors report no conflict of interest.

592 We are grateful to Dominique Barthés-Biesel and Claire Dupont (UMR CNRS 7338,
 593 Université de Technologie de Compiègne) for insightful discussions and for providing us
 594 their recent numerical data. We thank the NSF for support from CBET-2246791 and NIH
 595 via the National Heart, Lung, and Blood Institute under Grant No. R01HL132906.

REFERENCES

- 596 ACRIVOS, A. & LO, T. S. 1978 Deformation and breakup of a single slender drop in an extensional flow. *J.*
 597 *Fluid Mech.* **86**, 641–672.
- 598 BARTHÉS-BIESEL, D. 1980 Motion of a spherical microcapsule freely suspended in a linear shear flow. *J.*
 599 *Fluid Mech.* **100** (4), 831–853.
- 600 BARTHÉS-BIESEL, D. 1991 Role of interfacial properties on the motion and deformation of capsules in shear
 601 flow. *Physica A* **172** (1-2), 103–124.
- 602 BARTHÉS-BIESEL, D. 2016 Motion and deformation of elastic capsules and vesicles in flow. *Annu. Rev. Fluid*
 603 *Mech.* **48** (1), 25–52.
- 604 BARTHÉS-BIESEL, D., DIAZ, A. & DHENIN, E. 2002 Effect of constitutive laws for two-dimensional membranes
 605 on flow-induced capsule deformation. *J. Fluid Mech.* **460**, 211–222.
- 606 BARTHÉS-BIESEL, D. & RALLISON, J. M. 1981 The time-dependent deformation of a capsule freely suspended
 607 in a linear shear flow. *J. Fluid Mech.* **113**, 251–267.
- 608 BATCHELOR, G. K. 1970 Slender-body theory for particles of arbitrary cross-section in Stokes flow. *J. Fluid*
 609 *Mech.* **44**, 419–441.
- 610 BENTLEY, B. J. & LEAL, L. G. 1986 An experimental investigation of drop deformation and breakup in
 611 steady, two-dimensional linear flows. *J. Fluid Mech.* **167**, 241–283.
- 612 BOOTY, M. R. & SIEGEL, M. 2005 Steady deformation and tip-streaming of a slender bubble with surfactant
 613 in an extensional flow. *J. Fluid Mech.* **544**, 243–275.
- 614 BORKER, N. S. & KOCH, D. L. 2019 Slender body theory for particles with non-circular cross-sections with
 615 application to particle dynamics in shear flows. *J. Fluid Mech.* **877**, 1098–1133.
- 616 BUCKMASTER, J. 1973 The bursting of pointed drops in slow viscous flow. *J. Appl. Mech.* **40**, 18–24.
- 617 BUCKMASTER, J. D. 1972 Pointed bubbles in slow viscous flow. *J. Fluid Mech.* **55**, 385–400.
- 618 CHANG, K.-S. & OLBRICHT, W. L. 1993 Experimental studies of the deformation of a synthetic capsule in
 619 extensional flow. *J. Fluid Mech.* **250**, 587–608.
- 620 COX, R. G. 1970 The motion of long slender bodies in a viscous fluid. Part 1. General theory. *J. Fluid Mech.*
 621 **44**, 791–810.
- 622 DODSON III, W. R. & DIMITRAKOPOULOS, P. 2008 Spindles, cusps, and bifurcation for capsules in stokes
 623 flow. *Phys. Rev. Lett.* **101** (20), 208102.
- 624 DODSON III, W. R. & DIMITRAKOPOULOS, P. 2009 Dynamics of strain-hardening and strain-softening capsules

- 625 in strong planar extensional flows via an interfacial spectral boundary element algorithm for elastic
 626 membranes. *J. Fluid Mech.* **641**, 263–296.
- 627 DOWELL, E. H. & HALL, K. C. 2001 Modeling of fluid-structure interaction. *Annu. Rev. Fluid Mech.* **33** (1),
 628 445–490.
- 629 DUBASH, N. & MESTEL, A. J. 2007 Behaviour of a conducting drop in a highly viscous fluid subject to an
 630 electric field. *J. Fluid Mech.* **581**, 469–493.
- 631 DUPONT, C. & BARTHÉS-BIESEL, D. 2024 Private communication, UMR CNRS 7338, Université de
 632 Technologie de Compiègne.
- 633 EGGLETON, C. D. & POPEL, A. S. 1998 Large deformation of red blood cell ghosts in a simple shear flow.
 634 *Phys. Fluids* **10** (8), 1834–1845.
- 635 FRAENKEL, L. E. 1969 On the methods of matched asymptotic expansions. Part I: A matching principle.
 636 *Proc. Camb. Phil. Soc.* **65**, 209–231.
- 637 HINCH, E. J. & ACRIVOS, A. 1979 Steady long slender droplets in two-dimensional straining motion. *J. Fluid*
 638 *Mech.* **91** (03), 401–414.
- 639 KELLER, J. B. & RUBINOW, S. I. 1976 Slender-body theory for slow viscous flow. *J. Fluid Mech* **75** (04),
 640 705–714.
- 641 LI, X. Z., BARTHÉS-BIESEL, D. & HELMY, A. 1988 Large deformations and burst of a capsule freely suspended
 642 in an elongational flow. *J. Fluid Mech.* **187**, 179–196.
- 643 MIETKE, A., OTTO, O., GIRARDO, S., ROSENDAHL, P., TAUBENBERGER, A., GOLFIER, S., ULBRICHT, E., ALAND,
 644 S., GUCK, J. & FISCHER-FRIEDRICH, E. 2015 Extracting cell stiffness from real-time deformability
 645 cytometry: theory and experiment. *Biophys. J.* **109** (10), 2023–2036.
- 646 NAVOT, Y. 1998 Elastic membranes in viscous shear flow. *Phys. Fluids* **10** (8), 1819–1833.
- 647 OTTO, O., ROSENDAHL, P., MIETKE, A., GOLFIER, S., HEROLD, C., KLAUE, D., GIRARDO, S., PAGLIARA, S.,
 648 EKPENYONG, A., JACOBI, A. *ET AL.* 2015 Real-time deformability cytometry: on-the-fly cell mechanical
 649 phenotyping. *Nat. Methods* **12** (3), 199–202.
- 650 POZRIKIDIS, C. 1990 The axisymmetric deformation of a red blood cell in uniaxial straining stokes flow. *J.*
 651 *Fluid Mech.* **216**, 231–254.
- 652 POZRIKIDIS, C. 2003a Deformed shapes of axisymmetric capsules enclosed by elastic membranes. *J. Engng*
 653 *Math.* **45**, 169–182.
- 654 POZRIKIDIS, C., ed. 2003b *Modeling and Simulation of Capsules and Biological Cells*. London: Chapman
 655 & Hall.
- 656 RAMANUJAN, S. & POZRIKIDIS, C. 1998 Deformation of liquid capsules enclosed by elastic membranes in
 657 simple shear flow: large deformations and the effect of fluid viscosities. *J. Fluid Mech.* **361**, 117–143.
- 658 RHODES, D. & YARIV, E. 2010 The elongated shape of a dielectric drop deformed by a strong electric field.
 659 *J. Fluid Mech.* **664**, 286–296.
- 660 ROSENDAHL, P., PLAK, K., JACOBI, A., KRAETER, M., TOEPFNER, N., OTTO, O., HEROLD, C., WINZI, M.,
 661 HERBIG, M., GE, Y. *ET AL.* 2018 Real-time fluorescence and deformability cytometry. *Nat. Methods*
 662 **15** (5), 355–358.
- 663 SHERWOOD, J. D. 1981 Spindle-shaped drops in a viscous extensional flow. *Math. Proc. Camb. Philos. Soc.*
 664 **90** (3), 529–536.
- 665 SHERWOOD, J. D. 1991 The deformation of a fluid drop in an electric field: a slender-body analysis. *J. Phys.*
 666 *A* **24**, 4047–4053.
- 667 SKALAK, R., TOZEREN, A., ZARDA, R. P. & CHIEN, S. 1973 Strain energy function of red blood cell membranes.
 668 *Biophys. J.* **13** (3), 245–264.
- 669 STONE, H. A., LISTER, J. R. & BRENNER, M. P. 1999 Drops with conical ends in electric and magnetic fields.
 670 *Proc. Roy. Soc. London A* **455** (1981), 329.
- 671 TILLET, J. P. K. 1970 Axial and transverse Stokes flow past slender axisymmetric bodies. *J. Fluid Mech.*
 672 **44**, 401–418.
- 673 TORNBERG, A.-K. & SHELLEY, M. J. 2004 Simulating the dynamics and interactions of flexible fibers in
 674 Stokes flows. *J. Comp. Phys.* **196** (1), 8–40.
- 675 VAN DYKE, M. 1964 *Perturbation Methods in Fluid Mechanics*. New York: Academic Press.
- 676 WALTER, J., SALSAC, A.-V., BARTHÉS-BIESEL, D. & LE TALLEC, P. 2010 Coupling of finite element and
 677 boundary integral methods for a capsule in a stokes flow. *Int. J. Numer. Methods Eng.* **83** (7),
 678 829–850.
- 679 WANG, Y. & DIMITRAKOPOULOS, P. 2006 A three-dimensional spectral boundary element algorithm for
 680 interfacial dynamics in Stokes flow. *Phys. Fluids* **18** (8).

681 YARIV, E. & RHODES, D. 2013 Electrohydrodynamic drop deformation by strong electric fields: slender-body
682 analysis. *SIAM J. Appl. Math.* **73** (6), 2143–2161.